



# 1 The Pacific-Indian Ocean Associated Mode in CMIP5

## 2 Models

3 Minghao Yang, Xin Li\*, Weilai Shi, Chao Zhang, Jianqi Zhang

4 College of Meteorology and Oceanography, National University of Defense Technology, Nanjing,  
5 211101, China

6 Correspondence to: Xin Li (lixin\_atocean@sina.cn)

7

8 **Abstract.** The Pacific-Indian Ocean associated mode (PIOAM) is the product of the tropical air-sea  
9 interaction at the cross-basin scale and the main mode of ocean variation in the tropics.  
10 Evaluating the capability of current climate models to simulate the PIOAM and finding the  
11 possible factors that affect the simulation results are beneficial to obtain more accurate future climate  
12 change prediction. Based on 55-yr the Hadley Centre Global Sea Ice and Sea Surface Temperature  
13 (HadISST) reanalysis and the output data from twenty-one Coupled Model Intercomparison Project  
14 (CMIP) phase 5 (CMIP5) models, the PIOAM in these CMIP5 models is assessed. It is found that the  
15 explained variance of PIOAM in almost all twenty-one CMIP5 models are underestimated. Although all  
16 models reproduce the spatial pattern of the positive sea surface temperature anomaly in the eastern  
17 equatorial Pacific well, only one-third of these models successfully simulate the ENSO mode with the  
18 east-west inverse phase in the Pacific Ocean. In general, CCSM4, GFDL-ESM2M and CMCC-CMS  
19 have a stronger capability to capture the PIOAM than that of the other models. The strengths of the  
20 PIOAM in the positive phase in less than one-fifth of the models are slightly stronger, and very close to  
21 HadISST reanalysis, especially in CCSM4. The interannual variation of PIOAM can be measured by  
22 CCSM4, GISS-E2-R and FGOALS-s2. Further analysis indicates that considering the carbon cycle,  
23 resolving stratosphere, chemical process or increasing the horizontal resolution of the atmospheric model  
24 may effectively improve the performance of the model to simulate the PIOAM.

25

### 26 1. Introduction

27

28 As early as the 1960s, Bjerkness (1966, 1969) studied the phenomenon of El Niño-Southern  
29 Oscillation (ENSO). Since then, the impact of ENSO on global climate has become a major concern in  
30 climate research. ENSO in the Pacific Ocean is the strongest interannual signal of global climate change,  
31 and has been extensively studied by a large number of scholars, including its occurrence and development



32 mechanism (Wyrтки, 1975; Philander et al., 1984; Suarez and Schopf, 1988; Jin, 1997; Li and Mu, 1999;  
33 Li and Mu, 2000; Li, 2002), its evolution characteristics and its impact on global weather and climate  
34 (Bjerknes, 1966; Rasmusson and Wallace, 1983; Ropelewski and Halpert, 1987; Li, 1990; Webster and  
35 Yang, 1992; Zhou and Zeng, 2001; Mu and Duan, 2003; Mu et al., 2007; Zheng et al., 2007). At the end  
36 of the 20th century, an interannual climate anomaly characterized by a sea surface temperature anomaly  
37 (SSTA) of opposing sign in the western and eastern tropical Indian Ocean, known as the Indian Ocean  
38 dipole (IOD), was reported by Saji et al. (1999) and Webster et al. (1999) and was catalogued as one of  
39 the major ocean-atmosphere coupled phenomena. The SSTA in the tropical Indian Ocean subsequently  
40 has been widely studied, and a great deal of literature has discussed the causes and mechanisms of the  
41 IOD, as well as its weather and climate impacts (Li and Mu, 2001; Li et al., 2003; Saji and Yamagata,  
42 2003; Cai et al., 2005; Rao et al., 2007; Zheng et al., 2013; Wang and Wang, 2014).

43 IOD was initially thought to be generated only by independent air-sea interactions in the tropical  
44 Indian Ocean, but some studies have suggested that the tropical Indian Ocean SSTA in 1997/1998 was  
45 caused by the influence of the ENSO event in the Pacific Ocean on the surface wind field of the Indian  
46 Ocean through anti-walker circulation over the equator, thus causing the SSTA in the Indian Ocean (Yu  
47 and Rienecker, 1999). It has also been suggested that the east-west asymmetry anomaly of the Indian  
48 Ocean SSTA in 1997/1998 may contain the triggering process of ENSO (Ueda and Matsumoto, 2000).  
49 Li et al. (2002) showed that there is a significant negative correlation between the tropical Indian Ocean  
50 SSTA dipole event and the Pacific SSTA dipole event (similar to ENSO mode) using statistical analysis.  
51 Huang and Kinter (2002) also noted that there was a significant relationship between IOD in the Indian  
52 Ocean and ENSO in the Pacific Ocean.

53 The movements and changes of Earth's fluids (atmosphere and oceans) have a certain connection,  
54 and the change in tropical sea surface temperature (SST) should not be an isolated phenomenon. IOD in  
55 the Indian Ocean and ENSO in the Pacific Ocean, both as significant basin-scale signals, are supposed  
56 to be closely related and interact with each other. Although the type of relationship between ENSO and  
57 IOD has not yet been fully demonstrated, extensive research has shown that both SST and the air-sea  
58 systems in the Pacific Ocean and the Indian Ocean are closely linked (Klein and Soden, 1999; Li et al.,  
59 2008; Huang and Kinter, 2002; Li et al., 2003; Annamalai et al., 2005; Cai et al., 2019). The walker  
60 circulation anomaly induced by SSTA over the equatorial Pacific Ocean will cause a walker circulation



61 anomaly over the Indian Ocean, which could inspire the occurrence and development of IOD in the  
62 Indian Ocean driven by abnormal wind stress in the lower layer. On the other hand, Indonesian  
63 Throughflow also plays a role in the connection between ENSO and IOD. The cold (El Nino) or warm  
64 (La Nina) SST of the warm pool in the Pacific Ocean can cool or warm the SST in the eastern equatorial  
65 Indian Ocean through the Indonesian Throughflow, which is conducive to the establishment of a positive  
66 or negative phase of IOD.

67 Yang and Li (2005) found the first leading mode of the tropical Pacific-Indian SSTA reflecting the  
68 opposite phase characteristics of both the middle west Indian Ocean and equatorial middle east Pacific  
69 Ocean and both the eastern Indian Ocean and equatorial western Pacific Ocean, from which they  
70 proposed the concept of the Pacific-Indian Ocean associated mode (PIOAM), and noted that the PIOAM  
71 can better reflect the influence of the tropical SSTA on Asian atmospheric circulation. Yang et al. (2006)  
72 subsequently found that the influences of the PIOAM and the ENSO model on summer precipitation and  
73 climate in China were very different, and their numerical experiments also showed that the simulation  
74 results obtained by considering the PIOAM were more consistent with observation data. By analyzing  
75 the monthly thermocline temperature anomaly (TOTA) from 1958-2007 and the weekly sea surface  
76 height (SSH) anomaly from 1992-2011 in the tropical Pacific-Indian Ocean, Li et al. (2013) further found  
77 that the PIOAM are more obviously in the subsurface ocean temperature anomaly field, especially in the  
78 thermocline. Based on the simulation results of the LASG/IAP (State Key Laboratory of Numerical  
79 Modeling for Atmospheric Sciences and Geophysical Fluid Dynamics/Institute of Atmospheric Physics)  
80 Climate system Ocean Model (LICOM), version 2 (LICOM2.0) (Liu et al. 2012) and observation data,  
81 Li and Li (2017) proved that PIOAM is an important tropical Pacific-Indian Ocean SST variation mode  
82 that actually exists both in observation and simulation. Therefore, when studying the influence of SSTA  
83 in the Pacific and Indian oceans on weather and climate, the Pacific and Indian oceans should be  
84 considered as unified. Since the PIOAM is so important, how well do current climate models simulate  
85 it? To answer this question, the outputs from the climate system models for the Coupled Model  
86 Intercomparison Project (CMIP) phase 5 (CMIP5) were used for this research, from which we aim to  
87 provide a more complete evaluation of the PIOAM and try to find possible reasons that cause the  
88 simulation biases. In the following, Sect. 2 includes a brief description of the reanalysis dataset, CMIP5  
89 models, and the methods used in this study. Section 3 presents the assessments of the PIOAM in the



90 CMIP5 models. A conclusion and discussion are given in Sect. 4.

91

92 **2. Data and methods**

93

94 The reanalysis data from the Hadley Centre Global Sea Ice and Sea Surface Temperature (HadISST)  
 95 (Rayner et al., 2003) data set is used for this study. The data are monthly averaged data from 1951 to  
 96 2005 with a spatial resolution of  $1^\circ \times 1^\circ$ . Brief information for the 21 CMIP5 models used in this article  
 97 is provided in Table 1. Considering that output data resolutions vary between the models, we first  
 98 interpolated all data into a  $1^\circ \times 1^\circ$  grid to facilitate comparison between the models and HadISST  
 99 reanalysis.

100

101

Table 1. List of 21 selected CMIP5 climate models.

Model name	Modeling group	Oceanic resolution (lon×lat)
CanESM2 (Second Generation Canadian Earth System Model)	Canadian Centre for Climate Modeling and Analysis, Canada	256×192
CCSM4 (The Community Climate System Model, version 4)	NCAR, USA	320×384
CMCC-CESM (Centro Euro-Mediterraneo sui Cambiamenti Climatici (CMCC) Carbon Earth System Model)	CMCC, Italy	182×149
CMCC-CM (CMCC Climate Model)	CMCC, Italy	182×149
CMCC-CMS (CMCC-CM with a resolved stratosphere)	CMCC, Italy	182×149
CNRM-CM5 (Centre National de Recherches Météorologiques (CNRM) Coupled Global Climate Model, version 5)	CNRM, France	362×292
FGOALS-s2 (The Flexible Global Ocean-Atmosphere-Land System model, Spectral Version 2)	LASG, China	360×196
GFDL-ESM2M (Earth System Model of Geophysical Fluid Dynamics Laboratory (GFDL) with Modular Ocean Model, version 4)	GFDL, USA	144×90
GISS-E2-H (Goddard Institute for Space Studies (GISS) Model E version 2 (GISS-E2) with HYCOM ocean model)	NASA, USA	144×90
GISS-E2-H-CC (GISS-E2-H with carbon cycle)	NASA, USA	144×90
GISS-E2-R (GISS-E2 with Russell ocean model)	NASA, USA	144×90
GISS-E2-R-CC (GISS-E2-R with carbon cycle)	NASA, USA	144×90
HadCM3 (the third version of the Hadley Centre coupled model)	Met Office Hadley Centre, UK	288×144
HadGEM2-AO (Hadley Global Environment Model 2 (HadGEM2)-Atmosphere-Ocean)	Met Office Hadley Centre, UK	360×216
HadGEM2-CC (HadGEM2-Carbon Cycle)	Met Office Hadley Centre, UK	360×216
HadGEM2-ES (HadGEM2-Earth System)	Met Office Hadley Centre, UK	360×216
IPSL-CM5B-LR (Institut Pierre Simon Laplace Climate Model 5B (IPSL-CM5B)-Low Resolution)	IPSL, France	182×149
IPSL-CM5B-MR (IPSL-CM5B 5A-Medium Resolution)	IPSL, France	182×149



MIROC-ESM (Model for Interdisciplinary Research on Climate, Earth System Model)	Atmosphere and Ocean Research Institute (AORI), Japan	256×192
MIROC-ESM-CHEM (An atmospheric chemistry coupled version of MIROC-ESM)	AORI, Japan	256×192
NorESM1-M (Norwegian Climate Centre Earth System Model)	Norwegian Climate Centre, Norway	384×320

102

103 The PIOAM is determined according to the method of Ju et al. (2004) and Li et al. (2018), that is,  
104 the first leading mode of the tropical Pacific-Indian ocean SSTA is used to represent the PIOAM. Ju et  
105 al. (2004) used this method to analyze SSTA in the tropical Pacific-Indian Ocean in different seasons,  
106 and found the existence of PIOAM in all seasons with a contribution to total variance of more than 33%,  
107 indicating that the spatial distribution structure of PIOAM was stable.

108 Accounting for the intimate connection between the Pacific ENSO mode and the Indian Ocean  
109 dipole, Yang et al. (2006) argued that the PIOAM index (PIOAMI) can be defined as the respectively  
110 normalized east-west SSTA differences of the equatorial areas in the two oceans. As to the SSTA, the  
111 SSTA of ENSO is stronger than that in the equatorial Indian Ocean because of the larger Pacific basin;  
112 however, as to the influence of the SSTA on East Asia, a series of numerical experiments clearly indicate  
113 that the effect of SSTA forcing on the Indian Ocean is stronger than that of the eastern equatorial Pacific  
114 (Shen et al., 2001; Guo et al., 2002; Guo et al., 2004; Yang et al., 2006). Therefore, the PIOAMI is  
115 defined on the basis of the respective normalized dipoles in the Pacific and the Indian Ocean. According  
116 to the method of Yang et al. (2006), The PIOAMI is defined as follows:

117 
$$\text{PIOAMI} = \text{IOI} + \text{POI} \quad (1)$$

118 
$$\text{IOI} = \text{SSTA}(5^\circ - 10^\circ \text{ N}, 50^\circ - 65^\circ \text{ E}) - \text{SSTA}(10^\circ \text{ S} - 5^\circ \text{ N}, 85^\circ - 100^\circ \text{ E}) \quad (2)$$

119 
$$\text{POI} = \text{SSTA}(5^\circ \text{ S} - 5^\circ \text{ N}, 130^\circ - 80^\circ \text{ E}) - \text{SSTA}(5^\circ \text{ S} - 10^\circ \text{ N}, 140^\circ - 160^\circ \text{ E}) \quad (3)$$

120 where IOI and POI are the normalized Indian Ocean and Pacific Ocean indices, respectively.

121

### 122 3. Results

123

#### 124 3.1 Spatial pattern

125

126 Figure 1 depicts the spatial pattern of PIOAM in the selected 21 CMIP5 models and their differences  
127 compared to HadISST reanalysis (Fig. 1a). Figure 1.b shows the results of a multi-model ensemble  
128 (MME) that represents the mean of the results from all selected models. To better and objectively evaluate



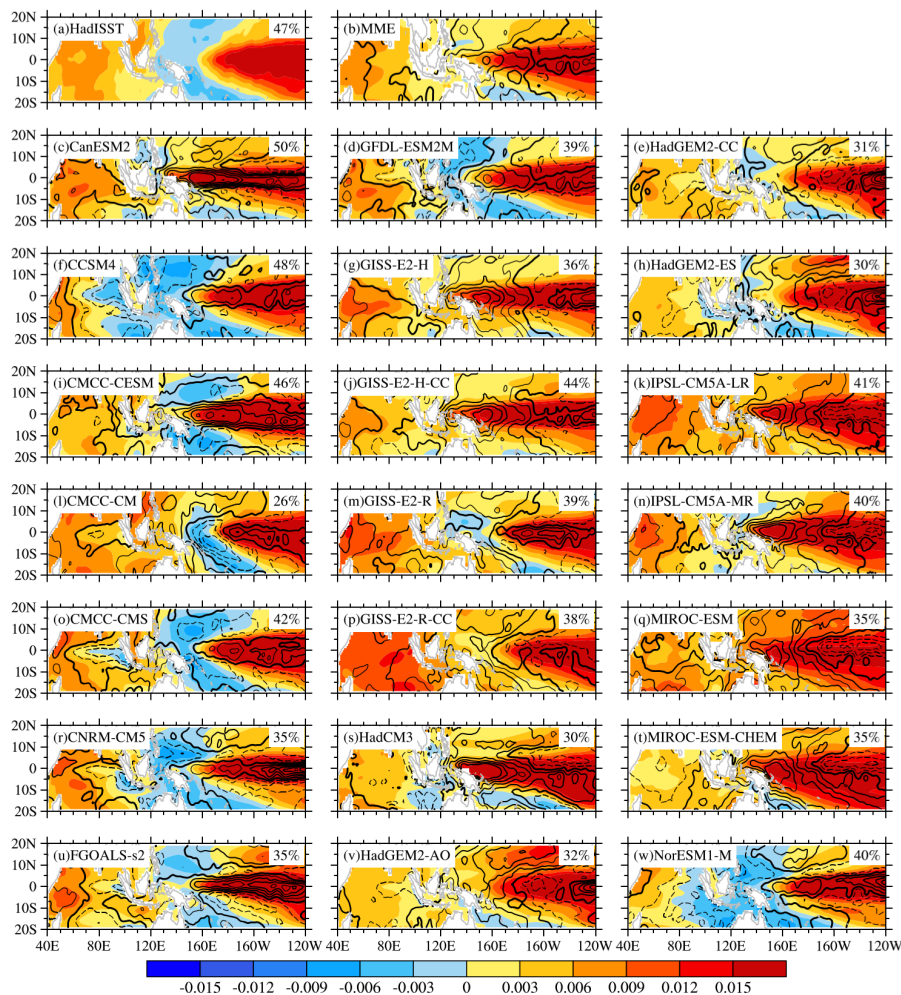
129 the capability of each model in simulating PIOAM, a Taylor diagram (Fig. 2) is also adopted to concisely  
130 display the relative information from multiple models, so that the differences among the simulations from  
131 all models are revealed clearly (Taylor, 2001; Jiang and Tian, 2013; Yang et al., 2018). According to  
132 HadISST reanalysis (Fig. 1a), with a 47% contribution to total variance, the PIOAM has a warm tongue  
133 spatial pattern in the eastern equatorial Pacific Ocean, whereas there is negative SSTA in the western  
134 equatorial Pacific Ocean, which exhibits an obvious ENSO mode in the Pacific Ocean. In addition, there  
135 are obvious positive SSTA in the western Indian Ocean region of the PIOAM, but the SSTA in the eastern  
136 equatorial Indian Ocean region remain positive. Considering that the so-called IOD is defined by the  
137 difference between the SSTA in the western equatorial Indian Ocean and that in the eastern equatorial  
138 Indian Ocean, this indicates zonal heat contrast of the Indian Ocean SSTA. Although it is called a dipole,  
139 it is not related to the mathematic meaning (Li et al., 2002; Yang et al., 2006). Therefore, it can be  
140 considered that the PIOAM presents an IOD mode in the Indian Ocean region.

141 Figure 1 shows that all of these models can generally reproduce the spatial pattern of PIOAM, yet  
142 large discrepancies exist regarding the strength, and the differences between the models are also  
143 significant. Except for the contribution to total variance of PIOAM in CCSM4 and CMCC-CESM are  
144 nearly consistent with HadISST reanalysis, the variance contribution of PIOAM in almost all CMIP5  
145 models are lower than those in the HadISST reanalysis, especially CMCC-CM with a contribution to  
146 total variance as small as 26%. In terms of strength, it is apparent that the simulation errors of these  
147 models are mainly concentrated in the Pacific Ocean compared to the Indian Ocean. Compared to the  
148 HadISST reanalysis, a majority of models overestimate the strength of PIOAM in the equatorial east  
149 Pacific and central Pacific; only one-seventh of the models (IPSL-CM5A-LR, IPSL-CM5A-MR and  
150 MIROC-ESM) underestimate the strength of PIOAM in the equatorial east Pacific, while the simulation  
151 results of HadGEM2-AO and CMCC-CM in the equatorial central Pacific and western Pacific are weak.  
152 The simulation errors of the strength of the ENSO mode in CCSM4, CMCC-CMS, GFDL-ESM2M and  
153 GISS-E2-R-CC are lower than those in other models. For the Indian Ocean, the strengths of PIOAM in  
154 only approximately one-quarter of the models (CanESM2, CMCC-CESM, GISS-E2-H-CC, HadCM3  
155 and HadGEM2-AO) are basically consistent with HadISST reanalysis with small simulation errors.  
156 Nearly half of the models were smaller for the eastern Indian Ocean, whereas more than half were larger  
157 for the western Indian Ocean. In general, the simulation error in the Indian Ocean region is significantly



158 smaller than that in the Pacific region. According to Fig. 2, it is apparent that the root mean square errors  
 159 (RMSEs) in MIROC-ESM-CHEM, IPSL-CM5A-LR and MIROC-ESM are relatively large, which  
 160 means that the capabilities of these modes to simulate the strength of PIOAM are still inadequate,  
 161 whereas the RMSEs in CCSM4, CMCC-CMS and GFDL-ESM2M are smaller than in other models with  
 162 a better performance. In addition, as shown in Fig. 1.b, MME better simulates the strength of PIOAM in  
 163 in the Indian Ocean region, but the simulation errors in the equatorial Pacific region are larger than that  
 164 of the HadISST reanalysis.

165



166

167 **Figure 1: PIOAM (shading) and the difference between each model and HadISST reanalysis (contour, with**  
 168 **an interval of 0.003, shown as black bold lines represent the contour with the zero value, unit: °C).**

169

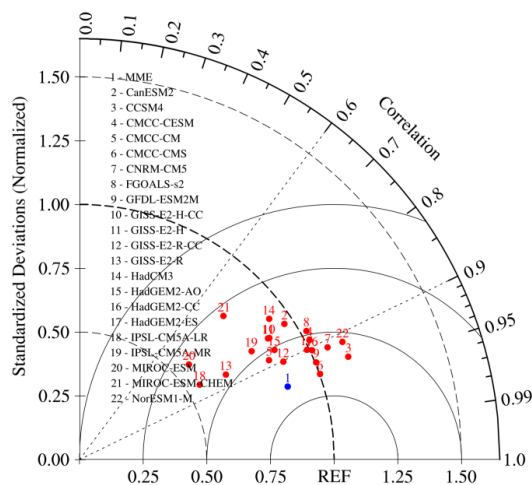


170 As for spatial patterns, the IOD mode in the Indian Ocean region can be simulated in almost all  
171 models except MIROC-ESM-CHEM. Although all these models reproduce the spatial pattern of the  
172 positive SSTA well in the eastern equatorial Pacific, only one-third of the models (CCSM4, CMCC-CM,  
173 CMCC-CMS, CNRM-CM5, FGOALS-s2, GFDL-ESM2M and NorESM1-M) successfully simulate the  
174 ENSO mode with the east-west inverse phase in the Pacific Ocean. In addition, the simulated positive  
175 SSTAs in the eastern equatorial Pacific in HadCM3 and MIROC-ESM-CHEM are further south.  
176 According to Fig. 2, more than one-third of these models (CCSM4, CMCC-CMS and GFDL-ESM2M,  
177 etc.) can simulate the spatial pattern of PIOAM well, and the spatial correlation coefficients between  
178 these models and the HadISST reanalysis are all greater than 0.9, especially CCSM4, which is as high as  
179 0.95. In contrast, the spatial pattern of PIOAM in MIROC-ESM-CHEM is unsatisfactory with a spatial  
180 correlation coefficient of only 0.69. The simulation results of HadCM3 and MIROC-ESM are also  
181 relatively poor, and the spatial correlation coefficients with HadISST reanalysis are less than 0.8. It can  
182 also be learned from Fig. 2 that, for the standard deviation of PIOAM, very large differences exist among  
183 these models. The standard deviations of PIOAM in IPSL-CM5A-LR, MIROC-ESM and GISS-E2-R-  
184 CC are quite different from those of the HadISST reanalysis, while the simulation results of CMCC-  
185 CMS, GFDL-ESM2M and HadGEM2-CC are basically close to those of the HadISST reanalysis and  
186 have better performance. It is noteworthy that the standard deviations of PIOAM in more than half of  
187 these models are smaller than that of the reanalysis, and their differences are large. Although the spatial  
188 pattern of PIOAM in MME is closer to the HadISST reanalysis and the RMSE is smaller than the vast  
189 majority of single models, the standard deviation of PIOAM in MME is smaller than that of the HadISST  
190 reanalysis.

191 In general, CCSM4, GFDL-ESM2M and CMCC-CMS have a stronger ability to simulate the  
192 PIOAM. In addition, although the MME of these models may not be as good as that of a single model in  
193 some specific aspects, overall, considering spatial pattern, standard deviation and RMSE, MME is still  
194 superior to most single models.

195





196

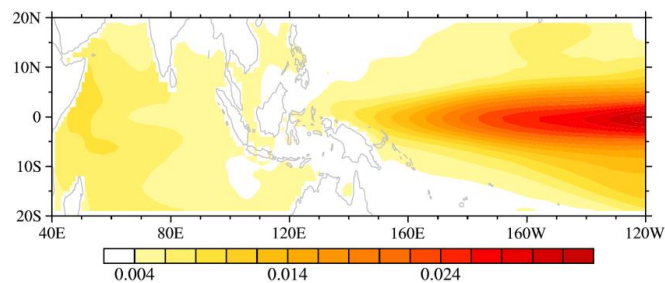
197 **Figure 2: Taylor diagrams of PIOAM.**

198

199

200 To further evaluate the differences between these models, Fig. 3 shows the distribution of standard  
 201 deviations between the CMIP5 models, which clearly reflects the regional differences between the  
 202 models. It is apparent that the differences are mainly concentrated in the eastern equatorial Pacific.  
 203 Therefore, the emphasis of improving the model on simulating the PIOAM is to improve the capability  
 204 of the model to simulate to the Eastern-Pacific (EP) type ENSO.

205



206

207 **Figure 3: The standard deviations of simulated PIOAM between the selected 21 CMIP5 models.**

208

### 209 3.2 PIOAM index

210

#### 211 3.2.1 Time series

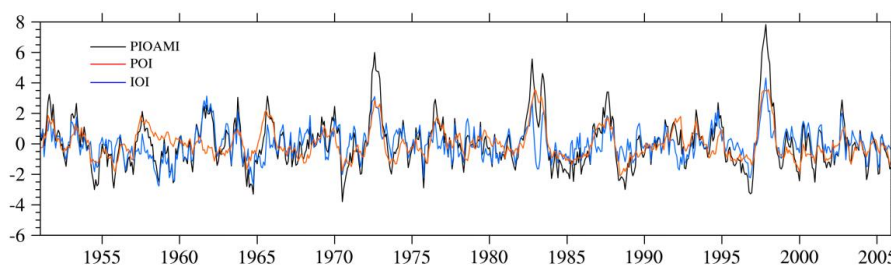
212

213 Figure 4. shows the monthly time series of the PIOAM index (PIOAMI), Pacific Ocean index (POI)  
 and Indian Ocean index (IOI) from 1951 to 2005. The wavelet analysis of PIOAMI indicates that PIOAM



214 has obvious seasonal and interannual variations, as well as interdecadal variations (feature is omitted).  
215 According to Fig. 4, POI and IOI have the same variation tendency at most times, thus the PIOAMI  
216 amplitude is greatly enhanced. However, there are a few cases where the two change in opposing ways,  
217 resulting in a much weaker PIOAMI. Moreover, from the time-series of PIOAMI, there is an interannual  
218 oscillation of positive and negative phases in the PIOAM, and there is also a phenomenon that the  
219 PIOAMI is very weak or not obvious in some years.

220



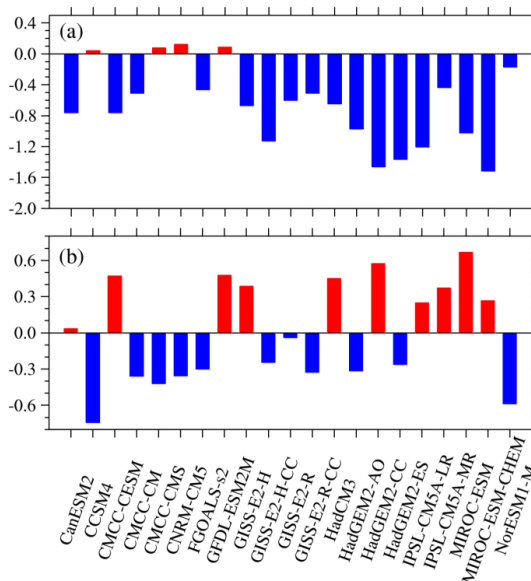
221

222 **Figure 4: Time-series of PIOAM index (black), Pacific Ocean index (red) and Indian Ocean index (blue) in**  
223 **the HadISST reanalysis.**

224

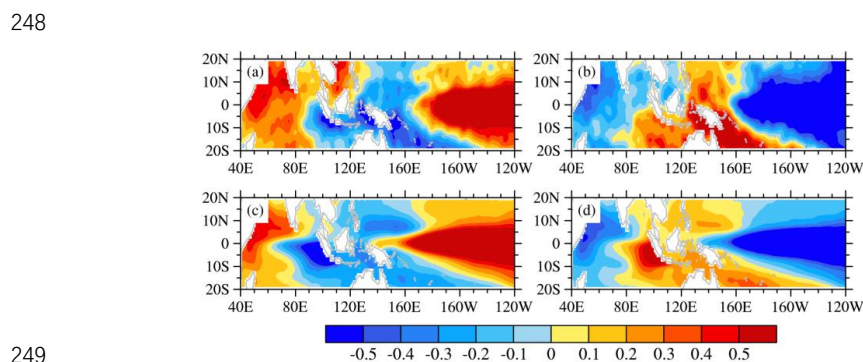
225 Considering that the PIOAM mainly reaches its peak in autumn, we select the year with significant  
226 positive and negative phases of PIOAM according to one standard deviation of PIOAMI in autumn, and  
227 calculate the difference in autumn PIOAMI between each model and the HadISST reanalysis (see Fig. 5)  
228 to further reveal the simulation of the CMIP5 models on the strength of the PIOAM. As shown by Fig.  
229 5.a, the simulated strengths of the PIOAM in the positive phase are underestimated in most models,  
230 whereas they are slightly overestimated in less than one-fifth of the models (CCSM4, CMCC-CMS,  
231 CNRM-CM5 and GFDL-ESM2M) are slightly stronger, which are very close to the HadISST reanalysis,  
232 especially in CCSM4. However, nearly half of the models overestimate the strength of the PIOAM in the  
233 negative phase (Fig. 5.b), in which the simulation results of CanESM2 and GISS-E2-R are consistent  
234 with the HadISST reanalysis. Although CCSM4 has a better performance in simulating the strength of  
235 the PIOAM in the positive phase than other models, the simulation error of the negative phase is very  
236 large.

237



238  
 239 **Figure 5: Difference in the amplitude of the PIOAMI in the positive phase (a) and negative phase (b) between**  
 240 **the CMIP5 models and HadISST reanalysis.**

241  
 242 According to PIOAM positive and negative phase year based on the autumn PIOAMI, SSTAs in  
 243 the tropical Pacific-Indian Ocean in October are composed to obtain the spatial pattern of SSTAs in the  
 244 PIOAM positive and negative phases. It is clear in Fig. 6 that the SSTAs in the Pacific-Indian Ocean in  
 245 both the MME of CMIP5 models and HadISST reanalysis present patterns with a tripole structure, where  
 246 the Indian Ocean is represented by the IOD mode and the Pacific Ocean by the ENSO mode, which again  
 247 demonstrates the authenticity of PIOAM and the rationality of PIOAMI used in this article.



249  
 250 **Figure 6: The tropical Pacific-Indian Ocean SSTAs of the PIOAM positive (a, c) and negative (b, d) phase in**  
 251 **October in the HadISST reanalysis (a, b) and the MME of CMIP5 models (c, d) (unit: °C).**  
 252

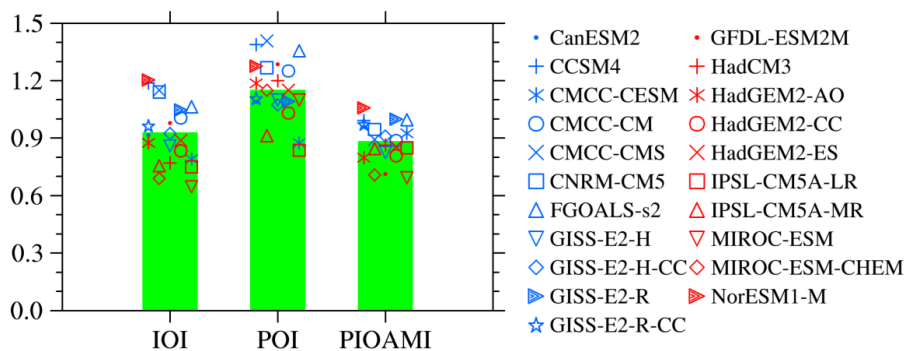


253 **3.2.2 Interannual Variation of PIOAM**

254

255 To evaluate the ability of these CMIP5 models to simulate the interannual variation of PIOAM, Fig.  
 256 7 shows the ratios of standard deviation of IOI, POI and PIOAMI in autumn in each model to those in  
 257 the HadISST reanalysis. It can be found that the difference in the simulation results of the interannual  
 258 variation of PIOAMI among these models is smaller compared to IOI and POI. The simulation results of  
 259 CCSM4, GISS-E2-R and FGOALS-s2 are almost consistent with HadISST reanalysis, indicating that  
 260 these three models have relatively strong capabilities to simulate the interannual variation of PIOAM.  
 261 Except that NorESM1-M overestimates the interannual variation of PIOAM, the simulation results in  
 262 most of the models are weak, especially MIROC-ESM, which leads to MME underestimating the  
 263 interannual variation of PIOAM compared to the HadISST reanalysis. In addition, the interannual  
 264 variations of IOI in GFDL-ESM2M, GISS-E2-R-CC and CMCC-CM are better than other models,  
 265 whereas the simulation results are underestimated in most models. In contrast to IOI, the vast majority  
 266 of models overestimate the interannual variations of POI, and the simulated interannual variations of POI  
 267 in only three models (IPSL-CM5A-MR, CMCC-CESM and IPSL-CM5A-LR) are weaker than the  
 268 HadISST reanalysis. Based on the above analysis, it is apparent that the interannual variation of PIOAM  
 269 is more closely to IOI than POI, and the interannual variation of PIOAM in autumn can be measured by  
 270 CCSM4, GISS-E2-R and FGOALS-s2.

271



272

273 **Figure 7: Ratios of standard deviation of autumn IOI, POI and PIOAMI in each model to those in the**  
 274 **HadISST reanalysis. Green bar represents the MME of the corresponding index.**

275

276 **3.2.3 The relationship of PIOAM with ENSO and IOD**

277

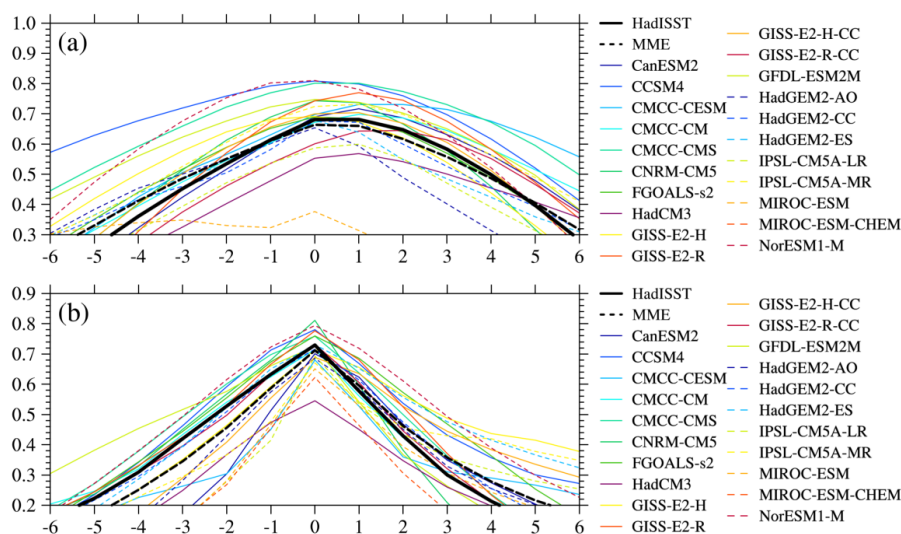
278 The lag-lead correlation analysis between PIOAMI and the Niño3.4 index derived from the



279 HadISST reanalysis shows that PIOAM has a close correlation with the ENSO mode at the same period  
280 and one month lagging with the correlation coefficient of 0.68 (Fig. 8.a). In addition, PIOAM and IOD  
281 also have a close correlation in the same period, with a correlation coefficient of 0.73 (Fig. 8.b), indicating  
282 that the PIOAM can reflect the activities of ENSO in the Pacific Ocean and IOD in the Indian Ocean to  
283 a considerable extent. In these CMIP5 models, more than one-half of the models successfully reproduce  
284 the maximum correlation between PIOAM and ENSO in the same period. The correlation coefficients  
285 of the PIOAMI and the Niño3.4 index in HadGEM2-AO and HadGEM2-ES are both 0.68, which is  
286 consistent with the HadISST reanalysis, and the correlation coefficients of FGOALS-s2, GISS-E2-H and  
287 GISS-E2-H-CC are 0.69, 0.69 and 0.70, respectively. However, the correlation coefficients of MIROC-  
288 ESM and MIROC-ESM-CHEM are only 0.37 and 0.30, which are significantly different from the results  
289 of the HadISST reanalysis and other models, indicating that the two models cannot simulate the close  
290 relationship between the PIOAM and ENSO well. In addition, the correlation coefficient of PIOAMI and  
291 the Niño3.4 index in MME is 0.66, which is slightly lower than the HadISST reanalysis but shows the  
292 close contemporaneity correlation between the PIOAM and ENSO; the overall change of the correlation  
293 coefficient series is very close to the HadISST reanalysis.

294 For the relationship between the PIOAM and IOD, it is apparent from the HadISST reanalysis in  
295 Fig. 8.b that the PIOAM and IOD show obvious close correlation in the same period, and the correlation  
296 coefficient is as high as 0.73. It is satisfactory that all selected CMIP5 models successfully reproduce the  
297 correlation between PIOAM and IOD in the same period, but the simulation results in more than half of  
298 them are underestimated. Among these models, the simulation results of HadGEM2-ES and GIS-E2-R-  
299 CC are basically consistent with the HadISST reanalysis, which shows that the two models have stronger  
300 capability to simulate the relationship between PIOAM and IOD.

301



302  
 303 **Figure 8: The lag-lead correlation coefficient of the PIOAMI with the Niño3.4 index (a) and IOD index (b).**  
 304 **Ordinate represents the correlation coefficient, and abscissa is the lag in months: positive (negative) for the**  
 305 **Niño3.4 index or IOD index (PIOAMI) leading PIOAMI (Niño3.4 index or IOD index)**  
 306

307 **4. Possible causes of simulation errors**

308  
 309 It is undoubtedly difficult to directly find the factors that influence the model to simulate the PIOAM.  
 310 However, the simulation results of model families, such as CMCC, IPSL, MIROC, GISS and HadGEM2,  
 311 provide comparative data to find the possible reasons that may lead to simulation differences. Using the  
 312 CMCC model family as an example, CMCC-CM is a climate model. Because of this, CMCC-CM,  
 313 CMCC-CESM and CMCC-CMS consider more complete physical processes and closer to the real world.  
 314 CMCC-CESM is a carbon earth system model, and CMCC-CMS is a climate model with a resolved  
 315 stratosphere. It can be found from Fig. 1. i, l and o that although CMCC-CM, CMCC-CESM and CMCC-  
 316 CMS all overestimate the strength of the PIOAM in the equatorial eastern Pacific Ocean, CMCC-CESM  
 317 also overestimates it in western Pacific Ocean, but CMCC-CM is weak. While the simulation results in  
 318 CMCC-CMS in the Pacific Ocean, especially the equatorial western Pacific Ocean, are better than that  
 319 in CMCC-CM and CMCC-CESM, but the strength of the PIOAM in the East Indian Ocean is weak in  
 320 CMCC-CMS. In addition, the variance contribution of PIOAM in CMCC-CESM is very close to that in  
 321 the HadISST reanalysis, reaching 46%, followed by CMCC-CMS with 42%, while CMCC-CM only has  
 322 26%. As shown in Fig. 2, not only is the spatial pattern of PIOAM in CMCC-CMS better with a higher  
 323 spatial correlation coefficient, the RMSE is smaller and the standard deviation of PIOAM is basically



324 consistent with the HadISST reanalysis. It can be found that considering the carbon cycle or resolving  
325 the stratosphere can effectively improve the capability to simulate the PIOAM.

326 Moreover, from the simulation results of GISS-E2-H and GISS-E2-H-CC, it can also be found that  
327 after considering the carbon cycle, GISS-E2-H-CC has no obvious improvement concerning the spatial  
328 pattern of PIOAM, and the RMSEs in GISS-E2-H and GISS-E2-H-CC are basically the same. However,  
329 the variance contribution of PIOAM in GISS-E2-H-CC is significantly improved compared to that in  
330 GISS-E2-H, ranging from 36% to 44%, which is closer to the HadISST reanalysis. Unlike GISS-E2-H  
331 and GISS-E2-H-CC, the variance contributions of PIOAM in GISS-E2-R and GISS-E2-R-CC are almost  
332 the same, but with a smaller RMSE, the spatial pattern and standard deviation of PIOAM in GISS-E2-  
333 R-CC are more consistent with the HadISST reanalysis than that in GISS-E2-R (see Fig. 2). Furthermore,  
334 in the HadGEM2 model family, HadGEM2-CC considers the carbon cycle on the basis of HadGEM2-  
335 AO. Compared to HadGEM2-AO, the RMSE of HadGEM2-CC is smaller, and the spatial type and  
336 standard deviation of PIOAM are more consistent with the HadISST reanalysis. Again, the performance  
337 of HadGEM2-CC effectively verifies the importance of the carbon cycle.

338 A comparison of the performance of MIROC-ESM and MIROC-ESM-CHEM revealed that the  
339 chemical process also has an obvious influence on the simulation results of PIOAM. After the chemical  
340 process is accounted for, the spatial standard deviation of PIOAM in MIROC-ESM-CHEM is closer to  
341 the HadISST reanalysis than that in MIROC-ESM, but the RMSE in MIROC-ESM-CHEM is slightly  
342 larger. The same is true for HadGEM2-E and HadGEM2-CC, indicating that the chemical process can  
343 effectively improve the simulation effect of the standard deviation of PIOAM.

344 In addition, it can be found from the two models from the IPSL-CM5A family (IPSL-CM5A-LR  
345 with low atmospheric resolution  $95\times 96$  and IPSL-CM5A-MR with medium atmospheric resolution  
346  $143\times 144$ ) that atmospheric resolution also affects the PIOAM simulation results. The RMSE in IPSL-  
347 CM5A-MR is slightly smaller than that in IPSL-CM5A-LR, and the spatial pattern of PIOAM is slightly  
348 better. Moreover, the simulated standard deviation of PIOAM in IPSL-CM5A-MR is much closer to the  
349 HadISST reanalysis than that in IPSL-CM5A-LR. This indicates that reasonably increasing the horizontal  
350 resolution of atmospheric model may also improve the simulation effect on PIOAM.

351

## 352 **5. Conclusion and discussion**

353



354 Based on HadISST reanalysis from 1951 to 2005, the Pacific-Indian Ocean associated mode,  
355 proposed by Yang and Li (2005) is evaluated for 21 CMIP5 models. This research provides a relatively  
356 comprehensive evaluation of the spatial pattern, the interannual variation and the relationship with ENSO  
357 and IOD of the PIOAM in the selected CMIP5 models. The main conclusions are as follows.

358 With a 47% contribution to total variance, the spatial pattern of PIOAM in the eastern equatorial  
359 Pacific Ocean is a warm tongue, whereas there is negative SSTA in the western equatorial Pacific Ocean  
360 that exhibits an obvious ENSO mode in the Pacific Ocean. In addition, the PIOAM presents an IOD  
361 mode in the Indian Ocean. The variance contributions of PIOAM in almost all CMIP5 models are smaller  
362 than that in the HadISST reanalysis. The simulation errors and differences among these models are  
363 mainly concentrated in the Pacific Ocean, compared to the Indian Ocean, and a majority of models  
364 overestimate the strength of PIOAM in the equatorial east Pacific and central Pacific. Although all these  
365 models reproduce the spatial pattern of the positive SSTA in the eastern equatorial Pacific well, only one-  
366 third of the models (CCSM4, CMCC-CM, CMCC-CMS, CNRM-CM5, FGOALS-s2, GFDL-ESM2M  
367 and NorESM1-M) successfully simulate the ENSO mode with the east-west inverse phase in the Pacific  
368 Ocean. In general, CCSM4, GFDL-ESM2M and CMCC-CMS have stronger capability to simulate the  
369 PIOAM than the other models.

370 The PIOAM is very weak or not obvious in some years and has obvious seasonal and interannual  
371 variations, as well as interdecadal variations. The simulated strengths of the PIOAM in the positive phase  
372 are underestimated in most models; only less than one-fifth of the models (CCSM4, CMCC-CMS,  
373 CNRM-CM5 and GFDL-ESM2M) are slightly stronger, and very close to the HadISST reanalysis,  
374 especially CCSM4. The interannual variation of PIOAM in CCSM4, GISS-E2-R and FGOALS-s2 are  
375 almost consistent with the HadISST reanalysis. Except that NorESM1-M overestimate the interannual  
376 variation of PIOAM, the simulation results in most models are weak, especially MIROC-ESM. The  
377 interannual variation of PIOAM in autumn can be measured by CCSM4, GISS-E2-R and FGOALS-s2.  
378 The PIOAM can well reflect the activities of ENSO in the Pacific Ocean and IOD in the Indian Ocean  
379 to a considerable extent with a close correlation to ENSO and IOD for the same period, as well as one  
380 month in advance with ENSO.

381 Considering the carbon cycle or resolving the stratosphere can effectively improve the capability of  
382 the model to simulate the PIOAM, a comparison of the performance of MIROC-ESM and MIROC-ESM-





383 CHEM revealed that the chemical process also has an obvious influence on the simulation results of  
384 PIOAM. The chemical process can effectively improve the simulation effect of the standard deviation of  
385 PIOAM. In addition, increasing the horizontal resolution of atmospheric model may improve the  
386 simulation effect on PIOAM as well.

387 Yang et al. (2006) found that only considering the ENSO in the Pacific cannot entirely  
388 explain the influence of SSTA on climate variation, and suggested that, to provide better  
389 scientific explanation for short-term climate prediction, the PIOAM and its influence should be  
390 considered and investigated. In addition, a review article by Cai et al. (2019) provides the first  
391 comprehensive review and summary of the current research advances in the interaction between  
392 the tropical Pacific-Indo-Atlantic climate systems, and they pointed out that an in-depth  
393 understanding of the dynamic mechanisms of intertropical basin interactions is an important  
394 way to improve the ability of seasonal to decadal climate prediction. Therefore, evaluating and  
395 improving the capability of current climate models to simulate the PIOAM and even the tropical  
396 Pacific-Indo-Atlantic climate systems are beneficial to obtain accurate climate change  
397 predictions. In addition, improving the level of climate prediction is not only helpful to grasp  
398 the changes in the ocean environment of the Pacific-Indian Ocean, but also propitious to  
399 improve the ability of prediction and assessment of ocean waves and wind energy (Zheng and  
400 Li, 2015; Zheng and Li, 2017).

401  
402 **Data availability.** The CMIP5 data are available at <https://esgf-node.llnl.gov/search/cmip5/>. The sea  
403 surface temperature are available at <https://www.metoffice.gov.uk/hadobs/hadisst/data/download.html>  
404

405 **Author contributions.** Xin Li and Weilai Shi conceived the idea and designed the structure of this  
406 paper; Minghao Yang performed the experiments; Minghao Yang, Chao Zhang and Jianqi Zhang  
407 analyzed the data; Minghao Yang wrote the paper.

408  
409 **Competing interests.** The author declares that they have no conflict of interest.

410  
411 **Author Contributions.** This research was supported by National Natural Science Foundation of China  
412 (4160501, 41490642, 41520104008).

413



414 References:

415

416 Annamalai, H., Xie, S. P., McCreary, J. P. and Murtugudde, R.: Impact of Indian Ocean Sea Surface  
417 Temperature on Developing El Niño. *J. Clim.*, 18(1), 302-319, doi:10.1175/jcli-3268.1, 2005.

418 Bjerknes, J.: A possible response of the atmospheric Hadley circulation to equatorial anomalies of  
419 ocean temperature, *Tellus.*, 18(4), 820-829, doi:10.3402/tellusa.v18i4.9712, 1966.

420 Bjerknes, J.: Atmospheric teleconnections from the equatorial Pacific, *Mon. Wea. Rev.*, 97(3), 163-  
421 172, doi:10.1175/1520-0493(1969)097<0163:atftpe>2.3.co;2, 1969.

422 Cai, W. J., Hendon, H. H. and Meyers, G.: Indian Ocean dipolelike variability in the CSIRO Mark  
423 3 coupled climate model, *J. Climate*, 18(10), 1449-1468, doi: 10.1175/jcli3332.1, 2005.

424 Cai, W., Wu, L., Lengaigne, M., Li, T., McGregor, Shayne., and et al.: Pan-tropical climate  
425 interactions, *Science*, 363(eaav4236), doi: 10.1126/science.aav4236, 2019.

426 Guo, Y. F., Zhao, Y. and Wang, J.: Numerical simulation of the relationships between the 1998  
427 Yangtze River valley floods and SST anomalies, *Adv Atmos Sci*, 19(3), 391-404,  
428 doi:10.1007/s00376-002-0074-0, 2002.

429 Guo, Y. F.: Numerical simulation of the 1999 Yangtze River valley heavy rainfall including  
430 sensitivity experiments with different anomalies, *Adv Atmos Sci*, 19(3), 391-404, doi:  
431 10.1007/BF02915677, 2004.

432 Huang, B. H. and Kinter, J. L.: Interannual variability in the tropical Indian Ocean, *J. Geophys. Res.*,  
433 107(C11): 3199. doi:10.1029/2001JC001278, 2002.

434 Jin, F. F.: An equatorial ocean recharge paradigm for ENSO. Part I: Conceptual model, *J. Atmos.*  
435 *Sci.*, 54(7), 811-829, doi:10.1175/1520-0469(1997)054<0811:aeorpf>2.0.co;2, 1997.

436 Ju, J. H., Chen, L. L. and Li, C. Y.: The preliminary research of Pacific-Indian Ocean sea surface  
437 temperature anomaly mode and the definition of its index, *Journal of Tropical Meteorology*  
438 (in Chinese), 20(6), 617-624, 2004.

439 Jiang, D. B. and Tian, Z. P.: East Asian monsoon change for the 21st century: results of CMIP3 and  
440 CMIP5 models, *Chinese Science Bulletin*, 58(12), 1427-1435, doi:10.1007/s11434-012-5533-  
441 0, 2012.

442 Klein, S. A. and Soden, B. J.: Remote sea surface temperature variation during ENSO: evidence for  
443 a tropical atmospheric bridge, *J. Clim.*, 12(4), 917-932, doi:10.1175/1520-  
444 0442(1999)012<0917:rsstvd>2.0.co;2, 1999.

445 Li, C. Y. Interaction between anomalous winter monsoon in East Asia and El Niño events, *Adv.*  
446 *Atmos. Sci.*, 7(1), 36-46, doi:10.1007/bf02919166, 1990.

447 Li, C. Y. and Mu, M. Q.: El Niño occurrence and sub-surface ocean temperature anomalies in the  
448 Pacific warm pool, *Chinese Journal of Atmospheric Sciences (in Chinese)*, 23(5), 513-521,  
449 1999.

450 Li, C. Y. and Mu, M. Q.: Relationship between East Asian winter monsoon, warm pool situation and  
451 ENSO cycle, *Chin. Sci. Bull.*, 45(16), 1448-1455, doi:10.1007/BF02898885, 2000.

452 Li, C. Y. and Mu, M. Q.: The influence of the Indian Ocean dipole on atmospheric circulation and  
453 climate. *Adv. Atmos. Sci.*, 18(5), 831-843. doi:10.1007/BF03403506, 2001.

454 Li, C. Y.: A Further Study of the Essence of ENSO, *Climate and Environmental Research (in*  
455 *Chinese)*, 7(2), 160-174, 2002.

456 Li, C. Y., Mu, M. Q., and Pan, J.: Indian Ocean temperature dipole and SSTA in the equatorial  
457 Pacific Ocean, *Chin. Sci. Bull.*, 47(3), 236-239, doi:10.1360/02tb9056, 2002.



- 458 Li, T., Wang, B., Chang, C. P. and Zhang, Y.: A theory for the Indian Ocean dipole-zonal mode, *J.*  
459 *Atmos. Sci.*, 60(17): 2119-2135, doi: 10.1175/1520-0469(2003)060<2119:atftio>2.0.co;2,  
460 2003.
- 461 Li, C. Y., Mu, M., Zhou, G. Q. and Yang, H.: Mechanism and prediction studies of the ENSO,  
462 *Chinese Journal of Atmospheric Sciences (in Chinese)*, 32(4), 761-781, 2008.
- 463 Liu, H., Lin, P., Yu, Y. and Zhang, X.: The baseline evaluation of LASG/IAP Climate system Ocean  
464 Model (LICOM) version 2, *Acta. Meteor. Sin.*, 26(3), 318-329, doi:10.1007/s13351-012-0305-  
465 y, 2012.
- 466 Li, X. and Li, C. Y.: The tropical pacific-indian ocean associated mode simulated by licom2.0, *Adv.*  
467 *Atmos. Sci.*, 34(12), 1426-1436, doi:10.1007/s00376-017-6176-5, 2017.
- 468 Li, C. Y., Li, X., Yang, H., Pan, J. and Li, G.: Tropical Pacific-Indian Ocean Associated Mode and  
469 Its Climatic Impacts *Chinese Journal of Atmospheric Sciences (in Chinese)*, 42(3), 505-523,  
470 2018.
- 471 Mu, M. and Duan, W. S.: A new approach to studying ENSO predictability: Conditional nonlinear  
472 optimal perturbation, *Chin. Sci. Bull.*, 48(10), 1045-1047, doi:10.1007/BF03184224, 2003.
- 473 Mu, M., Duan, W. S. and Wang, B.: Season-dependent dynamics of nonlinear optimal error growth  
474 and El Niño-Southern Oscillation predictability in a theoretical model, *Journal of Geophysical*  
475 *Research: Atmospheres*, 112(D10), doi:10.1029/2005JD006981, 2007.
- 476 Philander, S. G. H., Yamagata, T. and Pacanowski, R. C.: Unstable Air-Sea Interactions in the  
477 Tropics, *J. Atmos. Sci.*, 41(4), 604-613, doi: 10.1175/1520-  
478 0469(1984)041<0604:UASIT>2.0.CO;2, 1984.
- 479 Rasmusson, E. M. and Wallace, J. M.: Meteorological aspects of the El Niño/Southern Oscillation,  
480 *Science*, 222(4629), 1195-1202, doi:10.1126/science.222.4629.1195, 1983.
- 481 Ropelewski, C. F. and Halpert, M. S.: Global and regional scale precipitation patterns associated  
482 with the El Niño/southern Oscillation, *Mon. Wea. Rev.*, 115(8), 1606-1626, doi:10.1175/1520-  
483 0493(1987)1152.0.CO;2, 1987.
- 484 Rayner, N. A., Parker, D. E., Horton, E. B., Folland, C. K., Alexander, L. V., Rowell, D. P., Kent, E.  
485 C. and Kaplan, A.: Global analyses of sea surface temperature, sea ice, and night marine air  
486 temperature since the late nineteenth century, *J. Geophys. Res.*, 108(D14), 4407  
487 doi:10.1029/2002JD002670, 2003.
- 488 Rao, S. A., Masson, S., Luo, J. J., Behera, S. K. and Yamagata, T.: Termination of indian ocean  
489 dipole events in a coupled general circulation model, *J. Climate*, 20(13), 3018-3035,  
490 doi:10.1175/JCLI4164.1, 2007.
- 491 Suarez, M. J. and Schopf, P. S.: A delayed action oscillator for ENSO, *J. Atmos. Sci.*, 45(21), 3283-  
492 3287, doi: 10.1175/1520-0469(1988)045<3283:adaofe>2.0.co;2, 1988.
- 493 Saji, N. H., Coswami, B. N., Vinayachandran, P. N. and Yamagata, T.: A dipole in the tropical Indian  
494 Ocean, *Nature*, 401(6751), 360-363, doi:10.1038/43854, 1999.
- 495 Shen, X. S., Kimoto, M., Sumi, A., Numaguti, A. and Matsumoto, Jun.: Simulation of the 1998 East  
496 Asian Summer Monsoon by the CCSR/NIES AGCM. *J Meteor Soc Japan*, 79(3), 741-757,  
497 doi:10.2151/jmsj.79.741, 2001.
- 498 Saji, N. H. and Yamagata, T.: Possible impacts of Indian Ocean dipole mode events on global climate,  
499 *Climate Research*, 25(2), 151-169, doi: 10.3354/cr025151, 2003.
- 500 Taylor, K. E.: Summarizing multiple aspects of model performance in a single diagram, *Journal of*  
501 *Geophysical Research: Atmospheres*, 106(D7), 7183-7192, doi:10.1029/2000jd900719, 2001.



- 502 Ueda, H. and Matsumoto, J.: A possible triggering process of East–West asymmetric anomalies over  
503 the Indian Ocean in relation to 1997/98 El Niño, *J. Meteor. Soc. Japan*, 78(6), 803-818,  
504 doi:10.2151/jmsj1965.78.6\_803, 2000.
- 505 Wyrski, K.: El Niño-The Dynamic Response of the Equatorial Pacific Ocean to Atmospheric Forcing,  
506 *J. Phys. Oceanogr.*, 5(4), 572-584, doi:10.1175/1520-0485(1975)005<0572:entdro>2.0.co;2,  
507 1975.
- 508 Webster, P. J. and Yang, S.: Monsoon and ENSO: Selectively interactive systems. *Quart. J. Roy.*  
509 *Meteor. Soc.*, 118(507), 877-926, doi:10.1002/qj.49711850705, 1992.
- 510 Webster, P. J., Moore, A. M., Loschnigg, J. P. and Leben R. R.: Coupled ocean-atmosphere dynamics  
511 in the Indian Ocean during 1997-98, *Nature*, 401(6751), 356-360, doi: 10.1038/43848, 1999.
- 512 Wang, X. and Wang, C. Z.: Different impacts of various El Niño events on the Indian Ocean Dipole,  
513 *Climate Dyn.*, 42(3-4), 991-1005, doi: 10.1175/JCLI-D-12-00638.1, 2014.
- 514 Yu, L. S. and Rienecker, M. M.: Mechanisms for the Indian Ocean warming during the 1997-98 El  
515 Niño, *Geophys. Res. Lett.*, 26(6), 735-738, doi:10.1029/1999GL900072, 1999.
- 516 Yang, H. and Li, C. Y.: Effect of the Tropical Pacific-Indian Ocean Temperature Anomaly Mode on  
517 the South Asia High, *Chinese Journal of Atmospheric Science (in Chinese)*, 29(1): 99-110,  
518 2005.
- 519 Yang, H., Jia, X. L. and Li, C. Y.: The tropical Pacific-Indian Ocean temperature anomaly mode and  
520 its effect, *Chinese Science Bulletin*, 51(23): 2878-2884, doi:10.1007/s11434-006-2199-5, 2006.
- 521 Yang, M., Li, X., Zuo, R., Chen, X. and Wang, L.: Climatology and Interannual Variability of Winter  
522 North Pacific Storm Track in CMIP5 Models, *Atmosphere*, 9(3), 79,  
523 doi:10.3390/atmos9030079, 2018.
- 524 Zhou, G. Q. and Zeng, Q. C.: Predictions of ENSO with a coupled atmosphere–ocean general  
525 circulation model, *Adv. Atmos. Sci.*, 18(4), 587-603, doi:10.1007/s00376-001-0047-8, 2001.
- 526 Zheng, F., Zhu, J. and Zhang, R. H.: The impact of altimetry data on ENSO ensemble initializations  
527 and predictions, *Geophys. Res. Lett.*, 34(13), doi:10.1029/2007gl030451, 2007.
- 528 Zheng, X. T., Xie, S. P., Du, Y., Liu, L., Huang, G. and Liu, Q.: Indian Ocean Dipole Response to  
529 Global Warming in the CMIP5 Multimodel Ensemble, *J. Climate*, 26(16), doi:6067-6080,  
530 10.1175/JCLI-D-12-00638.1, 2013.
- 531 Zheng, C. W. and Li, C. Y.: Variation of the wave energy and significant wave height in the China  
532 Sea and adjacent waters. *Renewable and Sustainable Energy Reviews*, 43, 381-387,  
533 doi:10.1016/j.rser.2014.11.001, 2015.
- 534 Zheng, C. W. and Li, C. Y.: Propagation characteristic and intraseasonal oscillation of the swell  
535 energy of the Indian Ocean, *Applied Energy*, 197, 342-353,  
536 doi:10.1016/j.apenergy.2017.04.052, 2017.
- 537